THE AMERICAN SOCIETY OF MECHANICAL ENGINEERS
345 E. 47th St., New York, N.Y. 10017

98-GT-561

CONTROL OF SHOCK STRUCTURE AND SECONDARY FLOW FIELD INSIDE TRANSONIC COMPRESSOR ROTORS THROUGH AERODYNAMIC SWEEP

C. Hah
NASA Lewis Research Center
Cleveland, OH

S. L. Puterbaugh
Wright-Patterson AFB, Dayton, OH

A. R. Wadia
GE Aircraft Engines, Cincinnati, OH

ABSTRACT

The present paper reports a numerical study on the effects of aerodynamic sweep applied to a low-aspect-ratio, high-through-flow, state-of-the-art, axial transonic compressor design. Numerical analyses based on the Reynolds-averaged Navier-Stokes equations were used to obtain the performance of a conventional unswept rotor, a forward swept rotor, and an aft-swept rotor, at both design and off-design operating conditions. The numerical analyses predicted that the forward-swept rotor has a higher peak efficiency and a substantially larger stall margin than the baseline unswept rotor, and that the aft-swept rotor has a similar peak efficiency as the unswept rotor with a significantly smaller stall margin. The rig test confirmed the numerical assessment of the effects of aerodynamic sweep on the low-aspect-ratio, high-through-flow, transonic compressor rotor. Detailed analyses of the measured and calculated flow fields indicate that two mechanisms are primarily responsible for the differences in aerodynamic performance among these rotors. The first mechanism is a change in the radial shape of the passage shock near the casing by the endwall effect, and the second is the radial migration of low-momentum fluid to the blade tip region. Aerodynamic sweep can be used to control the shock structure near the endwall and the migration of secondary flows and, consequently, flow structures near the tip area for improved performance.

INTRODUCTION

Advanced designs for fans and compressors in aircraft engines aim to increase tip speed and blade loading beyond current state-of-the-art levels. However, large efficiency reductions occur in the tip region of transonic rotors when conventional design methods are extended beyond their originally intended range of flow conditions. This is due to the complex flow structures present in the tip region (passage shock, tip-clearance vortex, shock/boundary-layer interaction, shock/tip-clearance-vortex interaction, etc.).

The concept of swept rotors has been considered as a means of retaining aerodynamic efficiency at high rotor tip speed for highly loaded, high-through-flow transonic compressors (Wennerstrom and Puterbaugh [1984]). Although swept wing theory has been applied extensively for aircraft wing design, very few successful applications have been reported in compressor design until very recently. Most earlier studies of aerodynamic sweep for compressor designs (for example, Beatty, Savage, and Emery [1954], Smith and Yeh [1963], Lewis and Hill [1971], Gostelow and Smith [1968], Bliss et. al. [1976], Hayden et. al. [1978], etc.) applied aft-sweep to the blades and showed no convincing improvements in aerodynamic performance.

In the early 1980s, Prince [1980] observed that shock waves in low-aspect-ratio, low-hub-to-tip-ratio axial flow compressors were often quite three-dimensional in shape. It was noticed that the shock front was quite oblique to the flow in the spanwise direction even when a shock surface appeared normal to the relative flow in the cascade plane. Some compressor stages with oblique shock fronts had better efficiency than expected, and the pressure rises across the shocks were less than expected from the shock angles in the cascade plane. This observation led to the new three-dimensional shock loss model of Wennerstrom and Puterbaugh [1984]. Transonic compressors with aft-swept rotor blades were designed and tested in the early 1990s (Newbert, Hobbs, and Weingold [1990] and Rabe, Hoing, and Koff [1991]).

Presented at the International Gas Turbine & Aeroengine Congress & Exhibition
Stockholm, Sweden — June 2–5, 1998

The early design goal of the swept rotor was to reduce shock losses with an oblique shock shape in the meridional plane. Although some aft-swept transonic rotors showed improvements in efficiency, reduction in stall margin was almost always observed.

Earlier studies on forward-swept rotors in a low speed compressor showed that the sweep of the rotor can alter radial flow patterns on the blade suction surface, and that this can, in turn, improve the rotor performance (Mohammed and Prithviraj [1977] and Yamaguchi et al. [1991]). The application of forward sweep to transonic compressors was not seriously considered due to structural difficulties until G.E. Aircraft Engines and the U.S. Air Force started a cooperative research program on aerodynamic sweep applied to a low-aspect-ratio, high-through-flow transonic fan in 1988. The designs of an unswept rotor (Rotor 4), an aft-swept rotor (Rotor8), and a forward-swept rotor (Rotor9) were reported by Wadia, Szucs, and Crall [1997].

During test preparations and the manufacture of new swept rotors, it was decided to perform pre-test CFD studies of the new swept rotors (Rotor 8 and Rotor 9) along with Rotor 4. Complete rotor performance curves were calculated at 100 percent rotor speed. The CFD solutions predicted that the forward-swept rotor would have a higher rotor peak efficiency than the baseline unswept rotor. The numerical analysis also indicated that the forward-swept rotor has roughly a 30 percent larger stall margin than the unswept rotor. On the other hand, the aft-swept rotor showed approximately the same peak efficiency as the unswept rotor. The stall margin of the aft-swept rotor, however, was about 40 percent smaller than the baseline unswept rotor. The predicted superior performance of the forward-swept rotor was a surprise at the time and could not be adequately explained with traditional design tools. The performance of the forward-swept rotor was further numerically analyzed at partial rotor speeds.

Rotor running geometries at different rotor speeds were calculated with a structural analysis program and used in the numerical analyses. Deflections of rotor geometries at various rotor running speeds were therefore properly accounted for in the numerical simulations. All of the numerical solutions were obtained with a uniform tip clearance of 0.025 inches.

The objective of the present paper is to describe the detailed flow physics inside three transonic rotors with varying aerodynamic sweep using the numerical solutions obtained before the tests and the subsequently-obtained test results. The effects of aerodynamic sweep on aerodynamic efficiency and operating margin are discussed in detail in this paper.

ROTOR DESIGN AND TEST SETUP

The design and test results of the baseline unswept Rotor 4 have been reported by Hah and Puterbaugh [1991], Copenhaver, Hah, and Puterbaugh [1993], and Wadia and Copenhaver [1996]. Rotor 4 has excellent aerodynamic performance and stability. The key design parameters are given in Table 1. Rotor 4 was used as the technology standard to be improved upon through aerodynamic sweep. Figure 1 shows meridional views of the three rotors. Rotor 8 was swept aft through a combination of barreling the chord in the pitch region and leaning the blade tangentially opposite to the direction of rotation. Rotor 9 was swept forward using both chord barreling and tangential lean in the direction of rotation. Detailed descriptions of the design procedures for all of the rotors are given by Law and Wadia [1993] and by Wadia, Szucs, and Crall [1997]. The forward- and aft-swept rotors were

Table 1: Rotor 4 Key Design Parameters

Parameter	
Specific Flow	43.61 lbm/sec-ft^2
Corrected Tip Speed	1500 ft/sec
Stage Pressure Ratio	1.92
Inlet Corrected Flow	61.81 lb/sec
Measured Stage Efficiency	0.8764
Inlet Radius Ratio	0.312
Tip Diameter	17 in
Number of Blades	20
Mean Aspect Ratio	1.32
Average Solidity	2.3

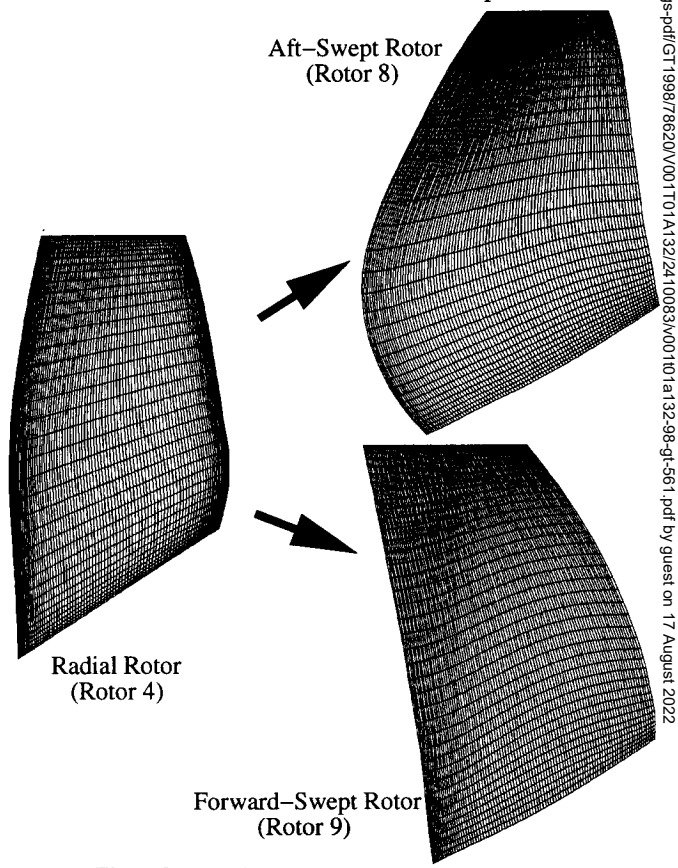

Fig. 1Comparison of rotor geometries.

designed for the same tip speed, inlet corrected flow, and pressure ratio requirements as the unswept rotor. Additionally, the two swept rotors were designed in such a way that performance changes are a consequence of aerodynamic sweep only. The three rotors were tested at the Compressor Aerodynamic Research Laboratory (CARL) at Wright Patterson Air Force Base (WPAFB) in a single-stage configuration. Figure 2 shows the test configuration. Details of the set-up, instrumentation, and experimental uncertainties are described by Law and Wadia [1993]. In addition to flow measurements at the stage inlet and exit, instrumentation for total pressure and total temperature at the vane leading edge were available. Rotor-alone performances were calculated with results from the stator leading edge instrumentation. Dynamic and steady pressure measurements along the rotor casing were obtained and compared with results from the numerical analyses.

It was found that the actual running clearance differed between rotors during the tests (Rotor 4: 0.025 inches; Rotor 8: 0.03 inches; Rotor 9: 0.022 inches). Each measured aerodynamic efficiency was therefore corrected for the variation of tip-clearance when compared with the numerical results. The correction was calculated using experimental data from a similar rotor with varying clearances (Wadia, Szucs, and Crall [1997]).

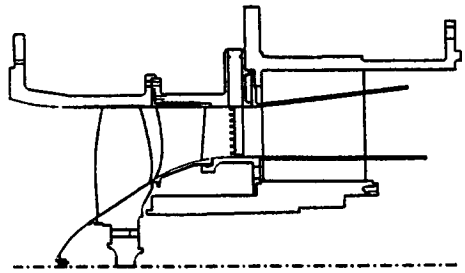

Fig. 2 Test configuration.

NUMERICAL PROCEDURE

For the current study, the governing equations are solved with a pressure-based implicit relaxation method using a fully conservative control volume approach. A third-order accurate interpolation scheme is used for the discretization of the convection terms and central differencing is used for the diffusion terms. The method is of second-order accuracy with smoothly varying grids. A standard two-equation turbulence model modified to include low-Reynolds-number effects near solid walls is applied for turbulence closure. Flow transition due to free stream turbulence structures can be modeled with the currently-applied turbulence model. Details of the current method, governing equations, and applications to transonic flows are given by Hah and Wennerstrom [1991].

The computational grid for Rotor 4 used in this study is shown in Figure 3. The grid was generated to give high orthogonality near the leading edge and near the blade surfaces where the most important flow phenomena (passage shock, shock-boundary layer interaction, etc.) occur. With this grid, spatial periodicity of grid points is not enforced at the periodic surfaces; instead, periodicity of flow properties is enforced inside the flow solver using an interpolation function. The grid consists of 51 nodes in the blade-to-blade direction, 51 nodes in the spanwise direction, and 152 nodes in the streamwise direction. As shown in Figure 3, 7 computational nodes are distributed across the blade tip and 7 nodes are located between the blade tip and the shroud to accurately describe the blade tip geometry. Precise modeling of the blade tip and clearance is necessary because very small changes in the tip clearance significantly affect the flow structures. The grids for Rotors 8 and 9 have the same dimensions and overall properties as the grid for Rotor 4.

Standard boundary conditions for transonic flow in a compressor are used (Hah and Wennerstrom [1991]). Approximately two Cray YMP single processor CPU hours are required to obtain a fully converged solution for a given operating condition.

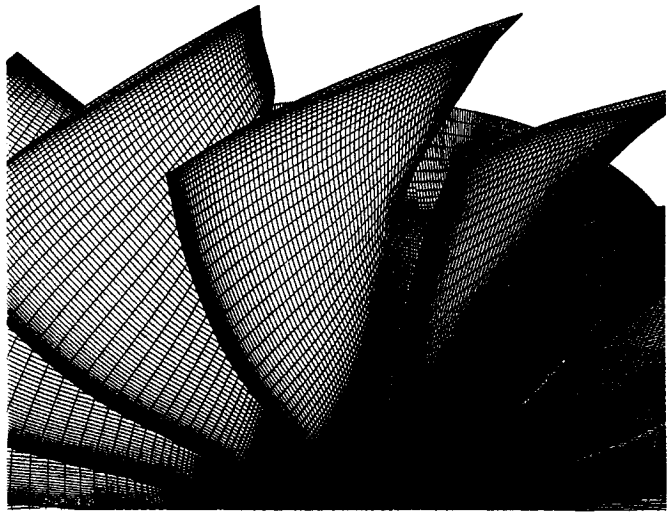

Fig. 3 Computational grid.

RESULTS AND DISCUSSION

Comparison of Aerodynamic Performance of Swept Rotors

The current numerical investigation is based on the numerical integration of the Reynolds-averaged Navier-Stokes equations. When the flow rate is reduced beyond a certain point by increasing the back pressure, the numerical solution does not converge to a steady mass flow; instead, the mass flow rate continues to decrease and the numerical integration eventually fails. These operating conditions are assumed to be beyond the fan operating range for the numerical analysis. The operating condition with the lowest mass flow rate that still yields a stable flow

field is considered to be the near-stall condition.

The numerically calculated rotor speed lines are compared with the rig test results in Figures 4 and 5. The pre-test calculations show very interesting comparisons. As shown in Figures 4 and 5, the forward-swept rotor has a higher pressure rise and a higher peak efficiency than the well-designed unswept rotor at the design speed. The forward-swept rotor also has roughly a 30 percent larger stall margin than the unswept rotor. The stall margin is defined as follows

$$SM = \left(\frac{PRS}{PR} \times \frac{W}{WS} - 1.0\right) \times 100$$

where PR and W are the pressure ratio and inlet corrected flow, respectively, on the same operating line, and PRS and WS are the pressure ratio and inlet corrected flow at stall. The peak efficiency of the aft-swept rotor is about the same as that of the unswept rotor at the design speed. However, the stall margin of the aft-swept rotor is approximately 40 percent less than that of the unswept rotor. The poor stall margin of the aft-swept rotor is in agreement with previously-reported characteristics of aft-swept transonic rotors (Neubert, Hobbs, and Weingold [1990]). As shown in Figures 4 and 5, the three rotors show quite different characteristics in their aerodynamic performance. As previously mentioned, the two swept rotors were designed to investigate the effects of aerodynamic sweep on performance. The design of the rotors was done in the early 1980s primarily using traditional compressor design tools. The three-dimensional viscous CFD analyses and the experimental results were obtained to verify the design intentions and to study changes in flow structure due to sweep.

Because the forward-swept rotor showed significant improvements in efficiency and stall margin over the unswept rotor, partial-speed performances were also investigated during the pre-test study. Rotor deflections at partial speeds were calculated and the calculated running geometries were used in the numerical analyses. The forward-swept rotor shows improvements in peak efficiency and stall margin compared to the unswept rotor at 90 percent rotor speed, similar to observations at the design rotor speed.

The forward- and aft-swept rotors were subsequently tested at the Compressor Aerodynamic Research Laboratory at the Wright-Patterson Air Force Base. The measured rotor performances are also shown in Figures 4 and 5, and verify the pre-test assessments of the relative performances of the swept rotors. At 100 percent rotor speed, differences in performance between the forward- and aft-swept rotors are very well predicted. Each numerical solution predicts roughly one-half point lower efficiency than the corresponding measurements. The currently-applied code predicts a slightly higher pressure rise than measured for each of the rotors, as shown in Figure 4. However, differences in pressure rise for different rotors are adequately predicted. At 90 percent rotor speed, the predictions show

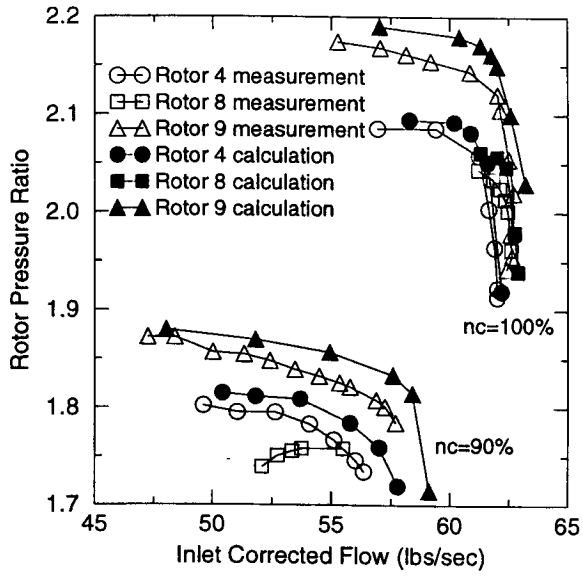

Fig. 4 Comparison of rotor pressure ratio.

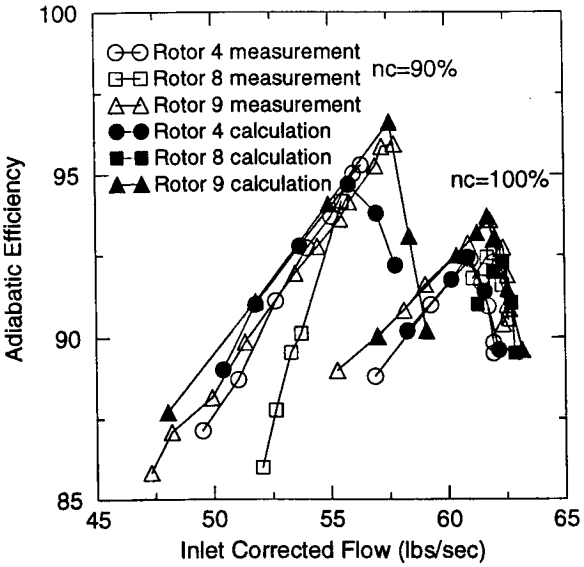

Fig. 5 Comparison of rotor adiabatic efficiency.

slightly better performance than the measurements. Again, however, the differences in aerodynamic performance between the unswept rotor and the swept rotors are properly estimated. Because of the limitations of the compressor test facility, measurements near the choke condition could not be obtained.

During the pre-test period and after the actual rig test, detailed studies were conducted to understand the fundamental flow physics responsible for the performance variation of the three rotors. The main objectives of the studies were to explain why the forward-swept rotor has a better peak efficiency and a significantly larger stall margin than the unswept rotor. In the following two sections, various findings which explain these two

phenomena are described.

Effects of Compressor Casing on Shock Structure Near the Endwall

As shown in Figure 1, aerodynamic sweep reaches a maximum near the shroud. The presence of the compressor casing has a major influence on the flow field through both inviscid and viscous effects as shown by Hah and Wennerstrom [1991]; the shock reacts to the presence of the casing by curving such that the shock surface becomes normal to the casing as the casing is approached. This is an inviscid effect which is considered in more detail later in this paper as it relates to backward and forward swept blading.

Calculated Mach number contours near the blade suction surfaces are shown in Figures 6 and 7. At both flow conditions, the shock front is nearly radial for the forward-swept rotor while slanting most for the aft-swept rotor. One interesting observation from the results in Figures 6 and 7 is that the radial shape of the shock front for the forward-swept rotor does not follow the direction of sweep. For all of the rotors, however, the shock becomes nearly normal to the casing in the outermost 10% of the span.

Calculated static pressure contours on the compressor casing are compared with ensemble-averaged high-frequency measurements in Figures 8 through 10. The calculated shock structures agree very well with the measurements, although the currently-applied CFD code predicts slightly higher pressure rises than measured. Changes in shock structure at different operating conditions, however, are very well predicted. At the peak efficiency condition for the unswept rotor, the passage shock is almost normal to the incoming flow. For the aft-swept rotor, the passage shock moves to the front of the rotor passage. For the forward-swept rotor, on the other hand, the passage shock is more oblique to the incoming flow, and the suction side leg of the shock is located roughly 60 percent chord downstream of the leading edge. At the near-stall condition for the aft-swept rotor, the passage shock is further detached from the leading edge. The same is true for the unswept rotor, as expected. For the forward-swept rotor, however, the passage shock is nearly normal to the inlet flow and sits at the entrance to the passage. Endwall flow structures shown in Figures 8 through 10 indicate that there are significant differences in the development of flow structures near the casing among the three rotors. The passage shock is located further upstream for the aft-swept rotor and further downstream for the forward-swept rotor than that for the unswept rotor. The passage shock moves upstream in the blade passage as the flow rate is decreased. When the passage shock moves further upstream of the leading edge, the flow field becomes unstable and the compressor cannot operate in a stable mode. The relative locations of the passage shock shown in Figures 8 through 10 indicate that the forward-swept rotor has a larger stall margin than the unswept rotor, while the aft-swept rotor has a smaller stall margin than the unswept rotor.

In the spanwise direction, the shock cannot intersect the outer casing obliquely. It must either turn normal to the casing or possibly bifurcate in a shock/boundary-layer interaction. Hah and Wennerstrom [1991] showed that the shock actually turns normal to the casing in a similar aft-swept transonic rotor. This requirement on the spanwise shock shape near the casing is an inviscid phenomenon. A simple illustration of the effect of the casing on the spanwise shock shape for simple swept rotors near the casing is given in Figure 11. In the absence of an endwall, the shock shapes for the forward- and aft-swept rotors would be similar. In the presence of the endwall, however, the shock must turn normal to the casing, moving upstream for the aft-swept rotor and downstream for the forward-swept rotor. When the shock moves upstream and detached from the blade passage, the incoming flow angle increases and the shock/boundary-layer interaction becomes stronger. The present swept rotors have a three-dimensional shape, and the shock structures away from the wall are not two-dimensional. However, the effect of the casing on the spanwise shock structure can be clearly observed on the endwall flow structures shown in Figures 6 through 10.

In Figure 12, inlet flow angles at the peak efficiency condition are compared for the three rotors at rotor design speed. Near the casing, the incoming flow angle is about 10 degrees higher for the aft-swept rotor than for the forward-swept rotor.

Radial distributions of pressure rise across the rotor and rotor adiabatic efficiency are compared in Figures 13 and 14. Typical of low-aspect-ratio transonic compressors, most of the aerodynamic loss occurs near the endwall for all three rotors. The main differences in performance between the three rotors also occurs near the endwall. Because the shocks all turn normal to the casing, no reduction in loss due to the oblique shock structure can be realized near the tip.

Distributions of normalized static pressure at the tip section and at the mid-span are compared in Figure 15. Results in Figure 15 show the relative locations of the passage shock very clearly. At the tip, the passage shock for the aft-swept rotor lies upstream of that for the unswept rotor, while the passage shock for the forward-swept rotor lies downstream. One very interesting observation from Figure 15 is that at mid-span, the passage shock for the forward-swept rotor lies upstream of that for the aft-swept rotor. This indicates that the aerodynamic loading is more evenly distributed in the spanwise direction for the forward-swept rotor. On the other hand, the loading is heavily concentrated near the tip for the aft-swept rotor.

In Figures 16 through 19, changes in the passage shock structure are compared as the compressor operating condition changes from peak-efficiency to near-stall. The changes in shock structure as the flow rate decreases indicate that the blade loading at the tip section rapidly increases for the unswept and aft-swept rotors. The flow structure at mid-span of these two rotors, however, seems to be stable in terms of passage shock location. This indicates that the flow near the tip section becomes unstable well

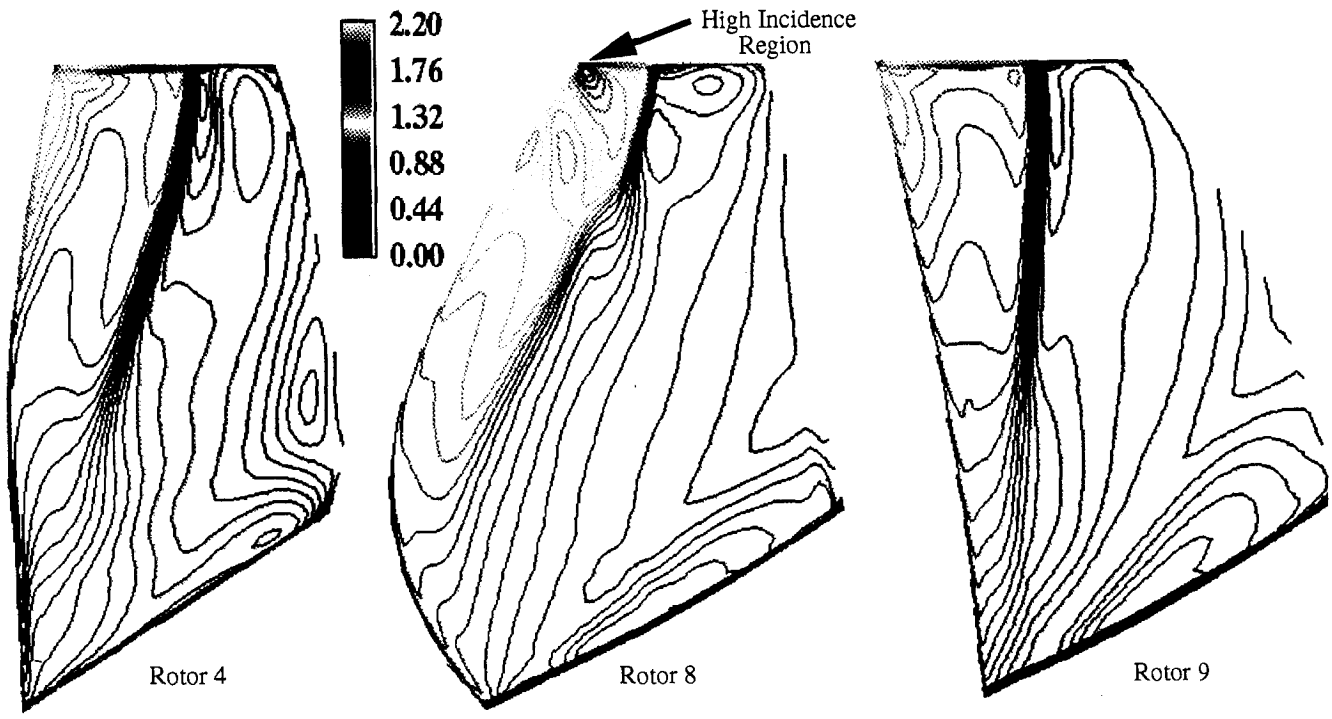

Fig. 6 Distribution of Mach number contours near suction surface at peak-efficiency condition.

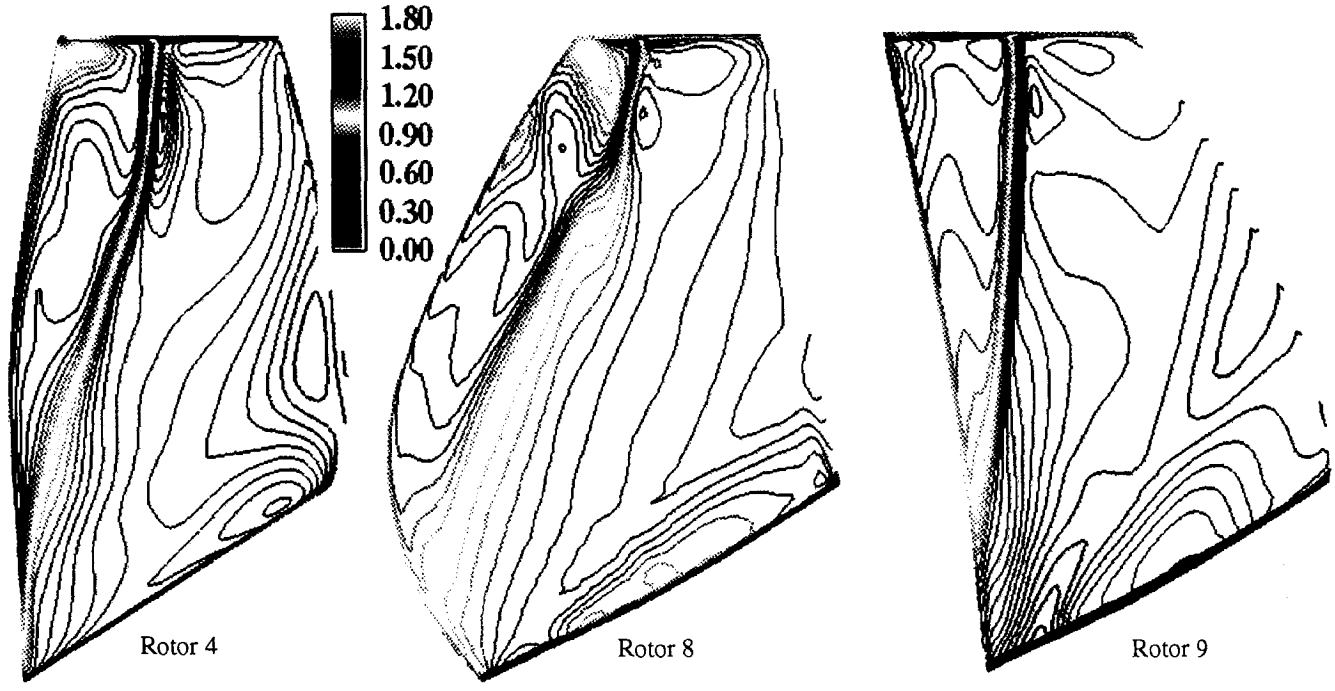

Fig. 7 Distribution of Mach number contours near suction surface at near-stall condition.

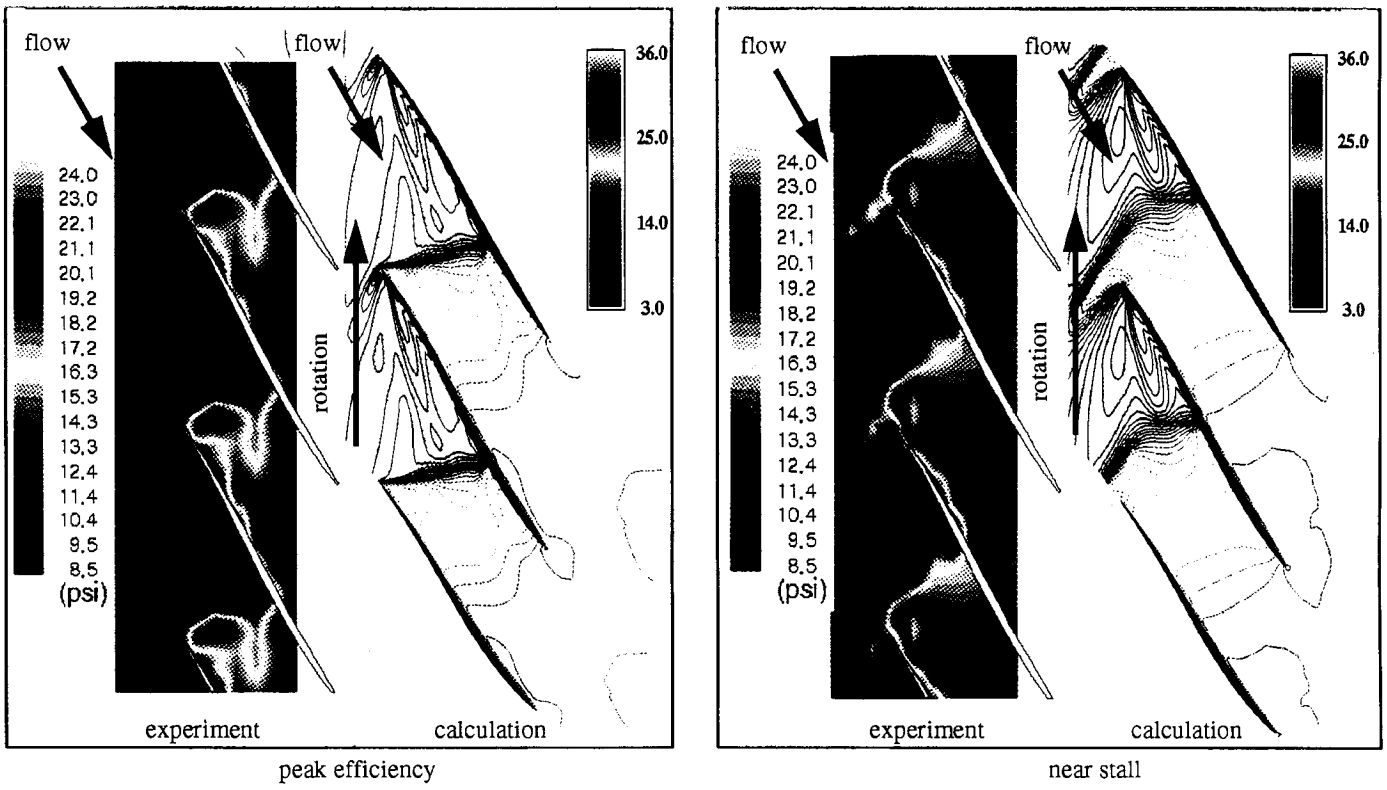

Fig. 8 Comparison of casing static pressure distribution for Rotor 4.

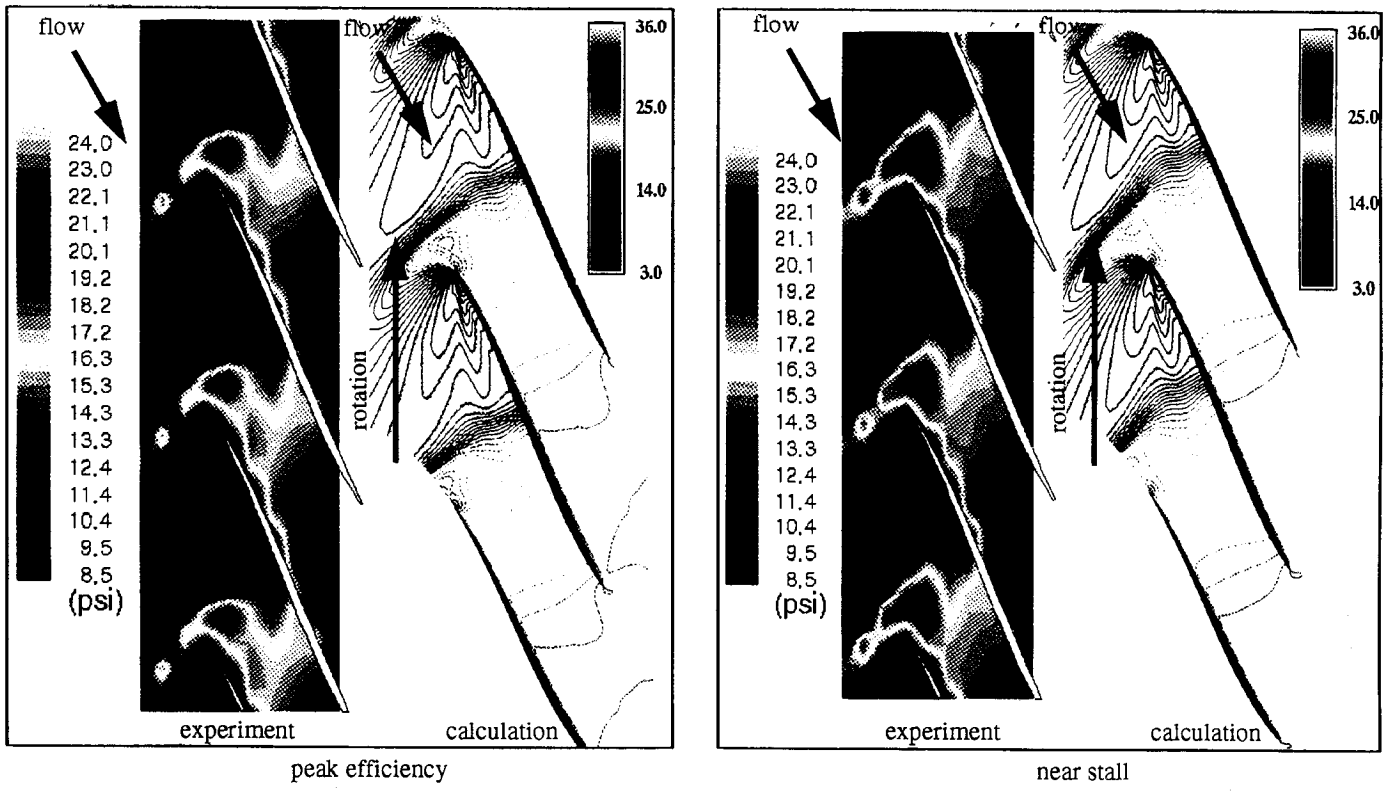

Fig. 9 Comparison of casing static pressure distribution for Rotor 8.

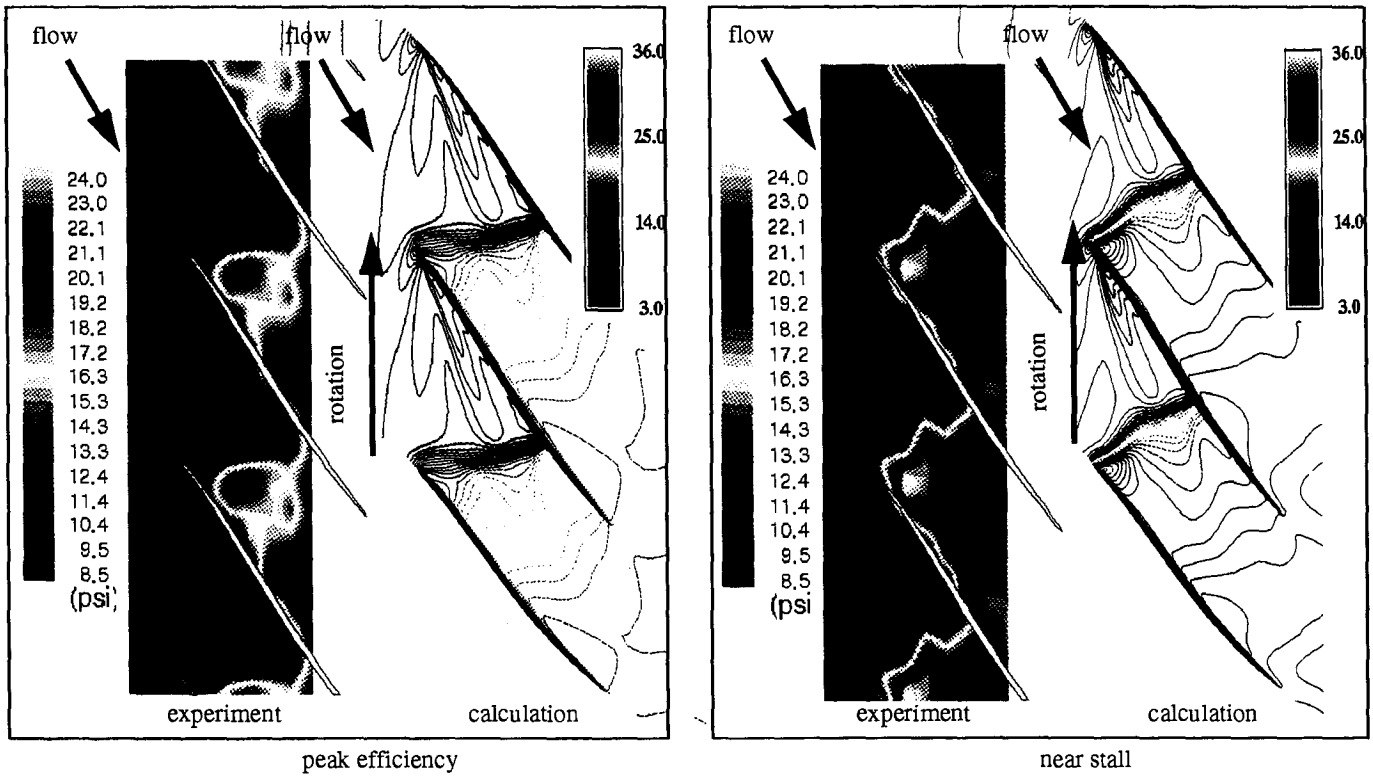

Fig. 10 Comparison of casing static pressure distribution for Rotor 9.

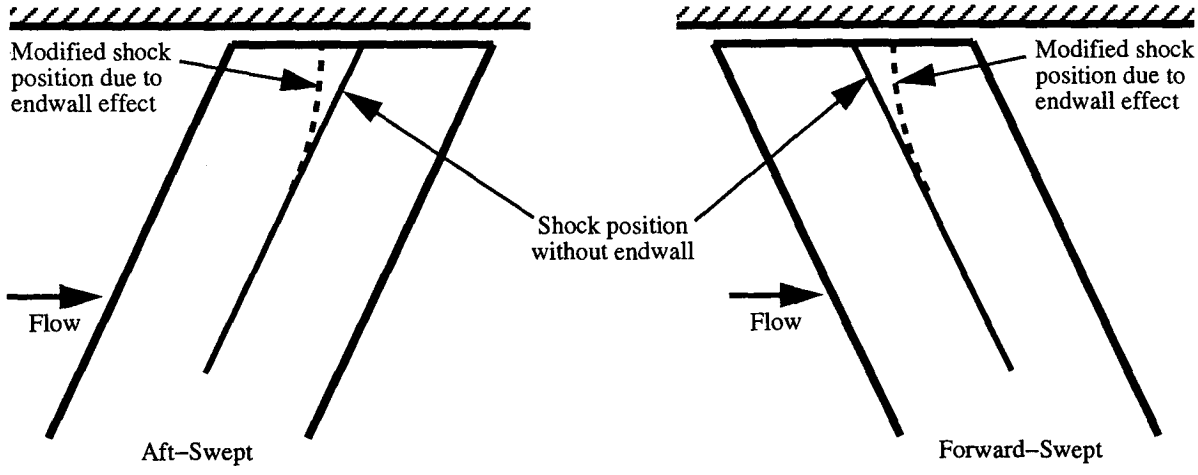

Fig. 11 Endwall effect on shock structure near the compressor casing.

before the rest of the flow for the unswept and aft-swept rotors. For the forward-swept rotor, on the other hand, the passage shock remains at the entrance to the blade passage at the tip section, even at the near-stall condition. At mid-span, however, the passage shock moves out in front of the blade passage, indicating a more evenly distributed aerodynamic loading for the forward-swept rotor at the near-stall condition. This even distribution of blade loading as the rotor approaches stall prevents premature stall at the tip and seems to be the main reason why the forward-swept rotor has a larger stall margin.

Velocity vectors colored with relative Mach number at the tip section of the blade are compared in Figure 19. The relative magnitudes of incidence angles and shock locations can be clearly compared in this figure. The region with low-momentum fluid due to the shock/tip-clearance-vortex interaction is located upstream of the leading edge for the aft-swept rotor, while this low-momentum region lies downstream of the leading edge for the forward-swept rotor. Since the aft-swept rotor has the highest

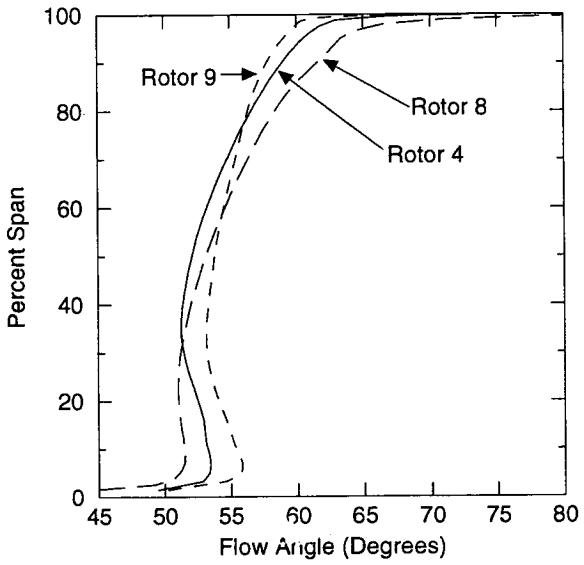

Fig. 12 Comparison of inlet flow angles.

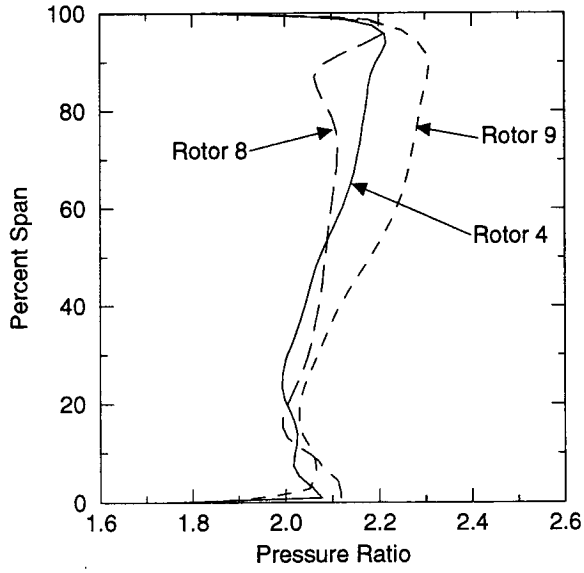

Fig. 13 Comparison of radial distribution of pressure ratio.

incidence, it also has the strongest shock. The resulting large shock losses and losses due to the strong shock/boundary-layer interaction are major causes for the poor aerodynamic performance of the aft-swept rotor. As shown in Figure 6, the passage shock quickly diffuses away from the endwall for the aft-swept rotor. This might contribute to the somewhat better efficiency of the aft-swept rotor near the mid-span. The flow structure near the casing of the aft-swept rotor contributes to its low efficiency and poor stall margin. As the passage shock turns normal to the casing near the endwall, it moves upstream and the incoming flow angle increases. The shock loss and shock/boundary-layer interaction then increase, which makes the flow field even more unstable. For the forward-swept rotor, the exact opposite phenomenon occurs due to the effect of the casing on the shock structure. The passage shock moves downstream in the passage as it turns normal to the casing, and the incoming flow incidence angle is reduced. The shock location at the near-stall condition for the forward-swept rotor shown in Figure 10 indicates that the flow near the tip is still stable and that the stall might be initiating away from the tip region.

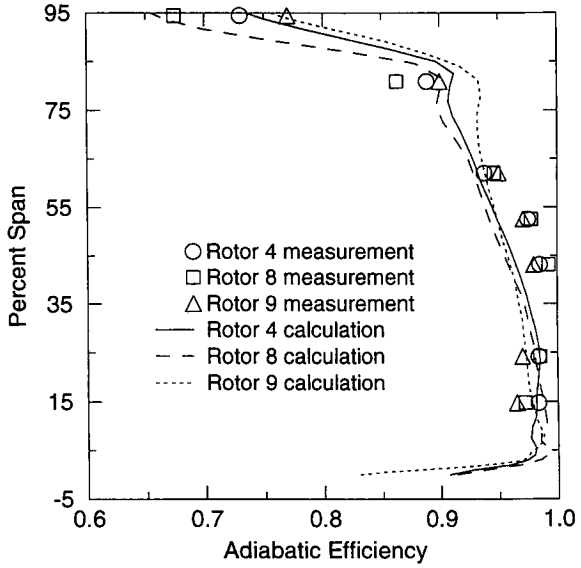

Fig. 14 Comparison of radial distribution of adiabatic efficiency.

Flow Structure Near the Blade Surface and Radial Flow Migration

The measured and the calculated spanwise distributions of adiabatic efficiency given in Figure 14 show that the forward-swept rotor is much more efficient in the outer half-span, while the aft-swept rotor is somewhat more efficient in the inner half-span. The forward aerodynamic sweep seems to improve the efficiency in the outer region of the compressor, while slightly reducing the efficiency in the inner region as compared to the original unswept rotor. For the aft-swept rotor, on the other hand, efficiency deteriorates substantially in the tip region and improves somewhat near the hub as compared to the unswept rotor.

Details of the flow structure near the blade suction surface and radial migration of the secondary flows were further examined to understand the differences in performance of the three rotors. Computed velocity vectors near the blade suction surfaces at the near-peak-efficiency condition are shown in Figure 20. Particle traces on the suction surface from the numerical solution are given in Figure 21. The local directions of secondary flow at mid-span are also shown in Figure 21 by the large hollow arrows. Inside the blade boundary layer, low-momentum fluid is forced to migrate toward the blade tip due to centrifugal force. For the aft-swept rotor, most of the centrifuged low-momentum fluid from the inner half-span of the blade ends up near the blade tip due to

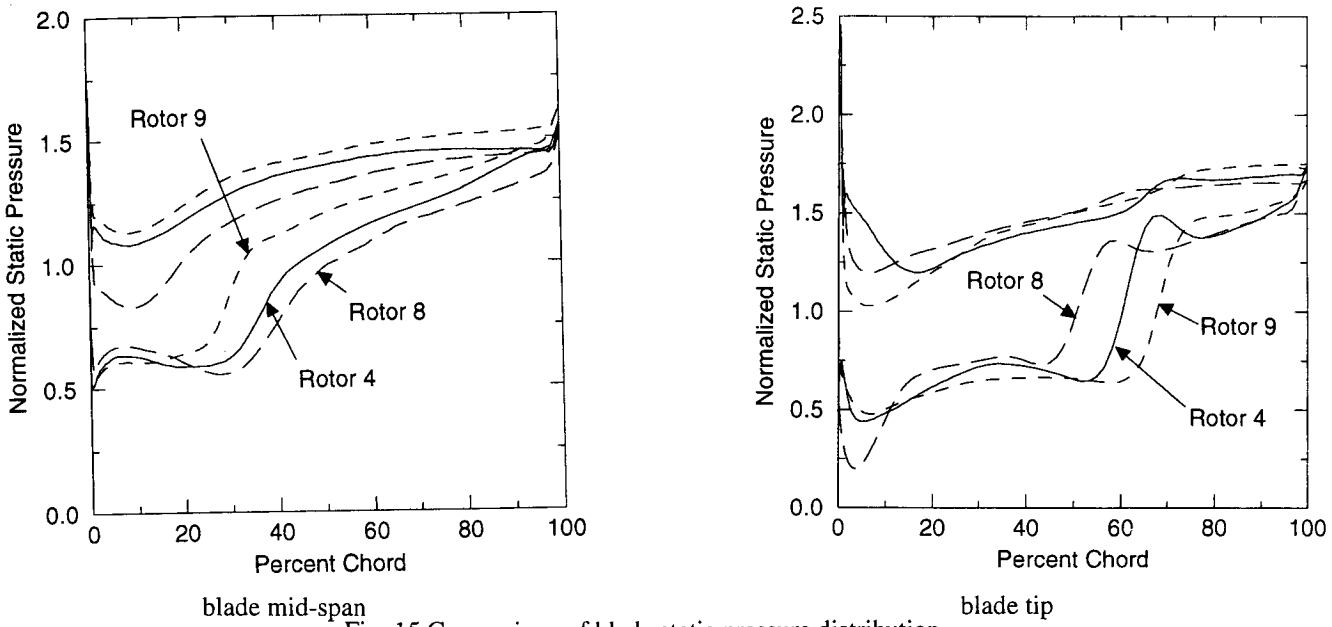

Fig. 15 Comparison of blade static pressure distribution.

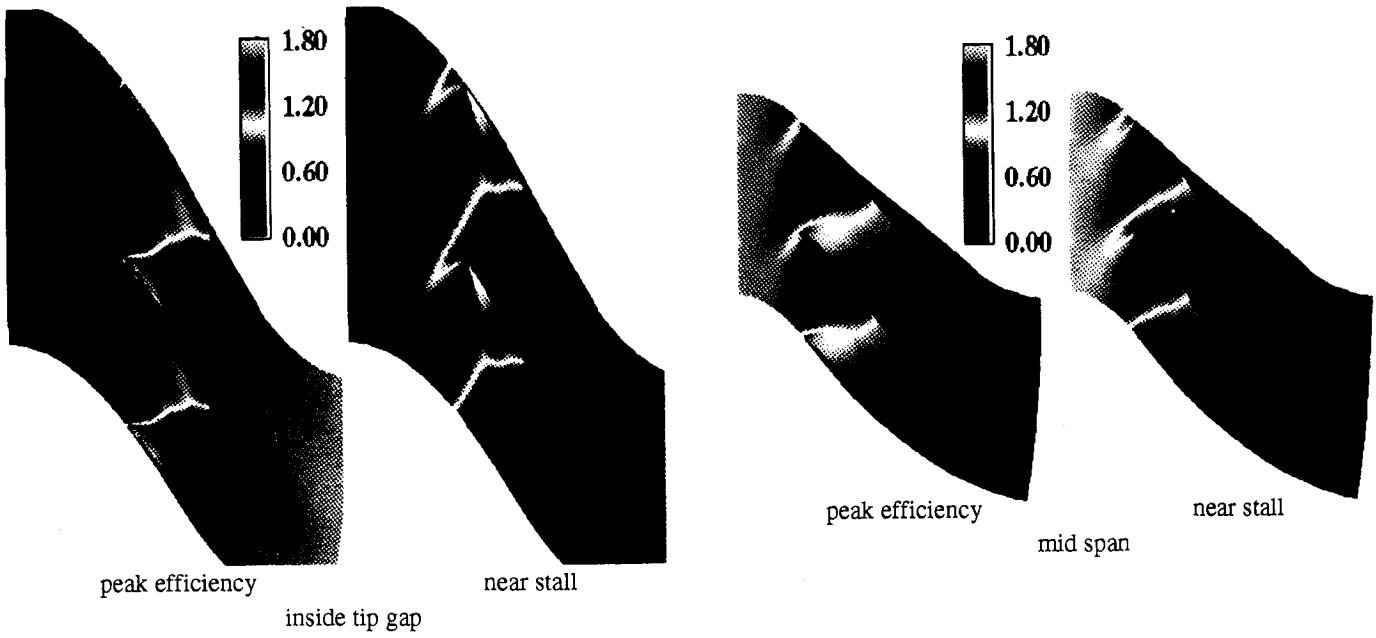

Fig. 16 Distribution of Mach number at mid-span and inside tip gap for Rotor 4.

the trailing edge profile, as shown in Figure 21. Large blockage in the tip region increases shock/boundary-layer interaction, pushing the passage shock further upstream and generating more aerodynamic loss. For the forward-swept rotor, low-momentum fluid centrifuged from the inner part of the blade exits the blade passage near the mid-span due to the direction of sweep and never reaches the tip section. The blockage near the tip section is therefore much smaller for the forward-swept rotor, and the passage shock stays inside the passage even at the near-stall condition. The behavior of secondary flows for the unswept rotor lies in between those of the two swept rotors.

In Figure 22, the distribution of entropy at mid-chord and at the rotor exit are compared among the three rotors. The entropy is computed from pressure and density nondimensionalized by the inlet values and specific heats nondimensionalized by the inlet gas constant. At mid-chord, entropy generation is concentrated near the tip section for all three rotors. The aft-swept rotor shows the largest loss at this location, as expected. The differences in entropy generation among the three rotors at mid-chord are primarily due to the differences in endwall shock strength, shock/boundary-layer interaction, and shock/tip-clearance-vortex interaction. The entropy distributions at the rotor exit show the effect of radial migration of secondary flows. On the suction surface, the generation of entropy is significantly larger for the aft-swept

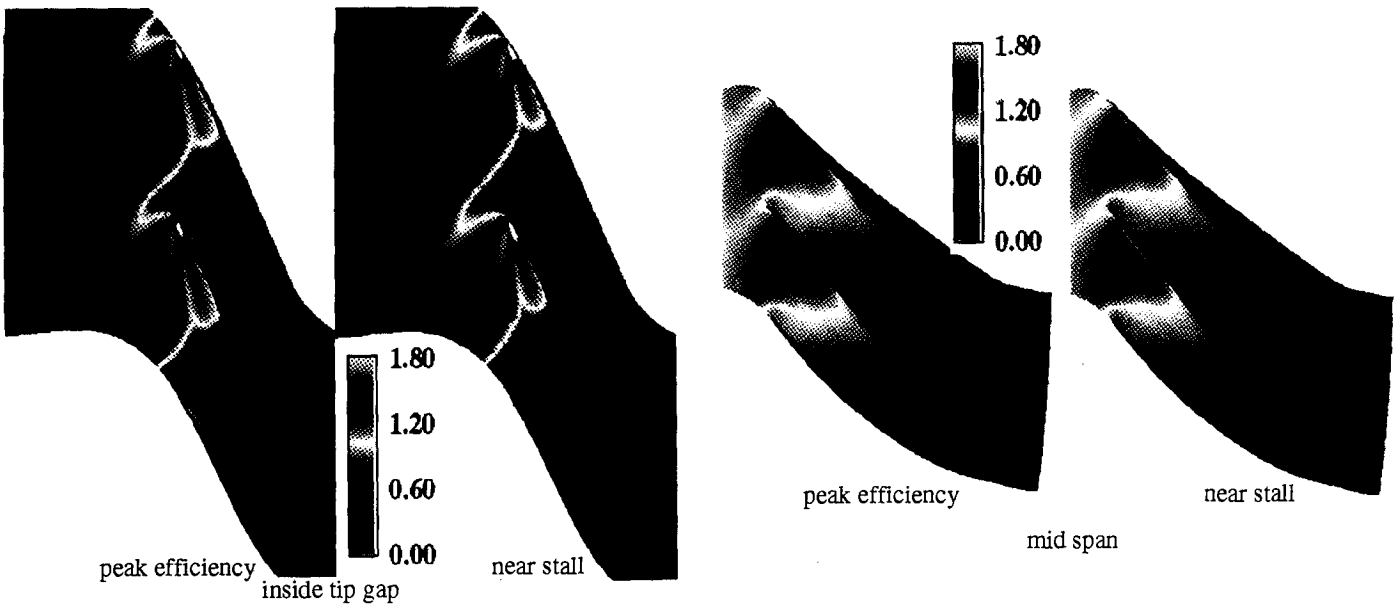

Fig. 17 Distribution of Mach number at mid-span and inside tip gap for Rotor 8.

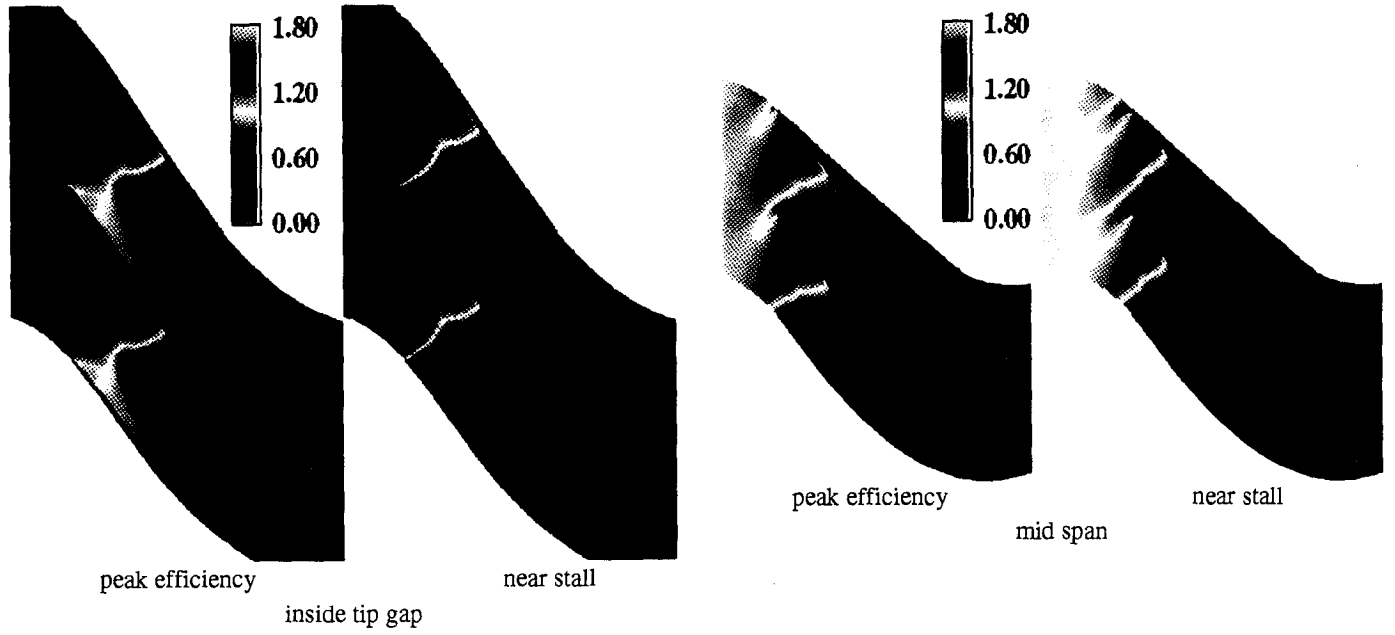

Fig. 18 Distribution of Mach number at mid-span and inside tip gap for Rotor 9.

rotor compared to the unswept and forward-swept rotors, which indicates that blade boundary layer growth tends to be largest for the aft-swept rotor. The radial migration of low-momentum fluid near the suction surface seems to be least for the forward-swept rotor. On the other hand, the tip clearance loss core for the forward-swept rotor, located at the corner of the blade pressure surface and the casing, seems larger in spanwise extent than for the other two rotors.

The results presented in this section indicate that aerodynamic sweep can be used to control the radial migration of secondary flows and high-entropy fluid, and subsequent flow blockage and shock/boundary-layer interaction. The reduction of inviscid shock losses due to three-dimensional shock sweep does not seem to be the primary loss-reduction mechanism for this type of transonic rotor. The performance of the blade tip region is crucial for efficient operation of these low-aspect-ratio, high-through-flow, axial transonic compressor rotors.

CONCLUDING REMARKS

The current study was performed in order to investigate the effects of aerodynamic sweep on a modern, low-aspect-ratio, high-through-flow, transonic axial compressor. A forward-swept

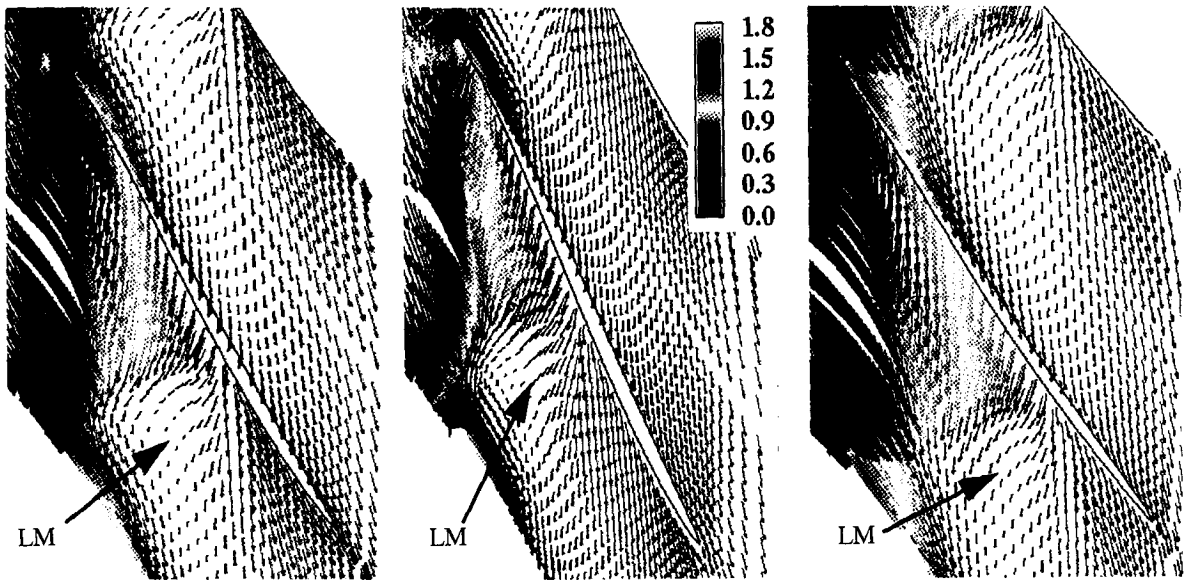

Fig. 19 Comparison of velocity vectors near rotor tip (colored by relative Mach number).

rotor and an aft-swept rotor were designed from a baseline unswept rotor which represents the state-of-the-art in design and performance of low-aspect-ratio, axial transonic rotors. Pre-test CFD analyses were performed for all three rotors to study differences in aerodynamic performance and flow structure. The pre-test CFD analyses showed that forward-sweep improves peak efficiency and produces a substantially larger stall margin. The analyses also indicated that aft-sweep produces no improvement in rotor peak efficiency. However, the stall margin of the aft-swept rotor was significantly lower than that of the unswept rotor. Subsequent rig tests validated the results drawn from the pre-test CFD analyses.

The results from the numerical analyses and the actual rig tests were further analyzed to understand the causes of the improved performance of the forward-swept rotor and the poor stall margin of the aft-swept rotor. The present study shows that two mechanisms are primarily responsible for the differences in aerodynamic performances among differently swept rotors. First, the radial shape of the passage shock must be normal to the compressor casing near the endwall. This condition forces the passage shock to move upstream in the blade passage near the tip for the aft-swept rotor. As the passage shock moves upstream in the blade passage, the incoming flow angle, the shock strength, and the shock/boundary-layer interaction all increase, resulting in larger aerodynamic losses and a poor stall margin. For the forward-swept rotor, the passage shock moves downstream in the passage as it turns normal to the casing and the shock/boundary-layer interaction becomes smaller. The other mechanism responsible for performance differences due to sweep is the migration of low-momentum fluid. The direction of blade sweep changes the amount of low-momentum fluid which migrates to and accumulates in the rotor tip region. Radial migration of low-momentum fluid to the tip region is least for the forward-swept rotor. Consequently, the passage-shock/boundary-layer interaction at the tip is substantially reduced, which results in higher overall aerodynamic efficiency. This accumulation of low-momentum fluid in the tip region, and corresponding aerodynamic blockage, is largest for the aft-swept rotor. Because of the reduced blockage at the tip for the forward-swept rotor, the flow near the tip remains stable even at the near-stall operating condition. As a result, it appears that the blade loading is maintained evenly across the span, which results in a larger stall margin.

The present study indicates that aerodynamic sweep can be used to optimize the shock structure near the casing, to control the transport and distribution of low-momentum fluid along blade surfaces, and consequently to control the shock/boundary-layer interaction in a transonic compressor. Therefore, the design of modern, low-aspect-ratio, high-through-flow, axial transonic compressors can be optimized with proper aerodynamic sweep. A CFD code based on the three-dimensional Reynolds-averaged Navier-Stokes equations has been successfully applied to perform pre-test analyses on the effects of aerodynamic sweep for a modern, low-aspect-ratio, axial transonic compressor. The differences in aerodynamic performance due to variations in sweep were adequately predicted. Such a numerical tool can be applied to design optimization with aerodynamic sweep.

ACKNOWLEDGEMENTS

The authors would like to acknowledge the contribution of J. Loellbach and F. Tsung of ICOMP at NASA Lewis Research Center in preparing the illustrations. We are also grateful to the management at G.E. Aircraft Engines, USAF, and NASA for giving us permission to publish the current work.

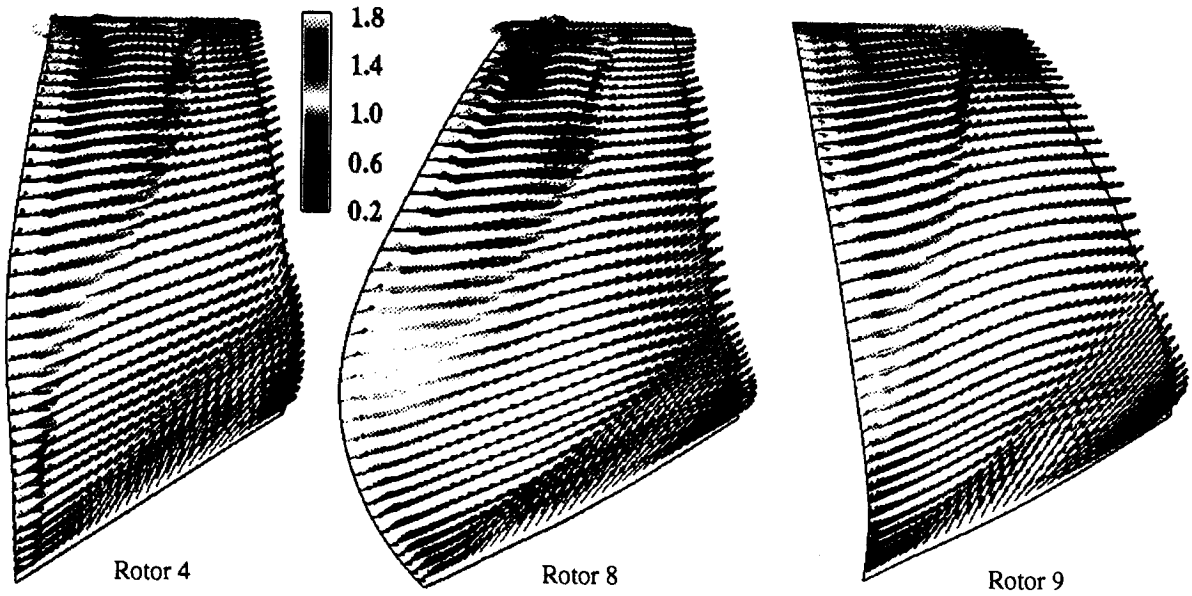

Fig. 20 Comparison of velocity vectors near suction surface at design speed near peak-efficiency (colored by relative Mach number).

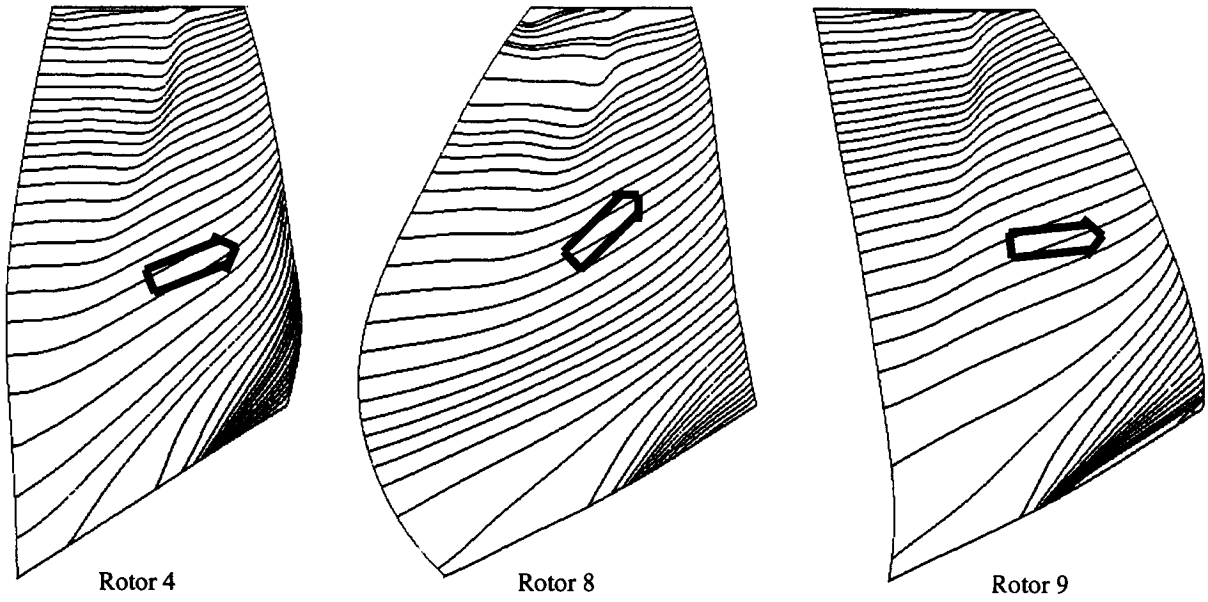

Fig. 21 Particle traces near suction surface at design speed near peak-efficiency.

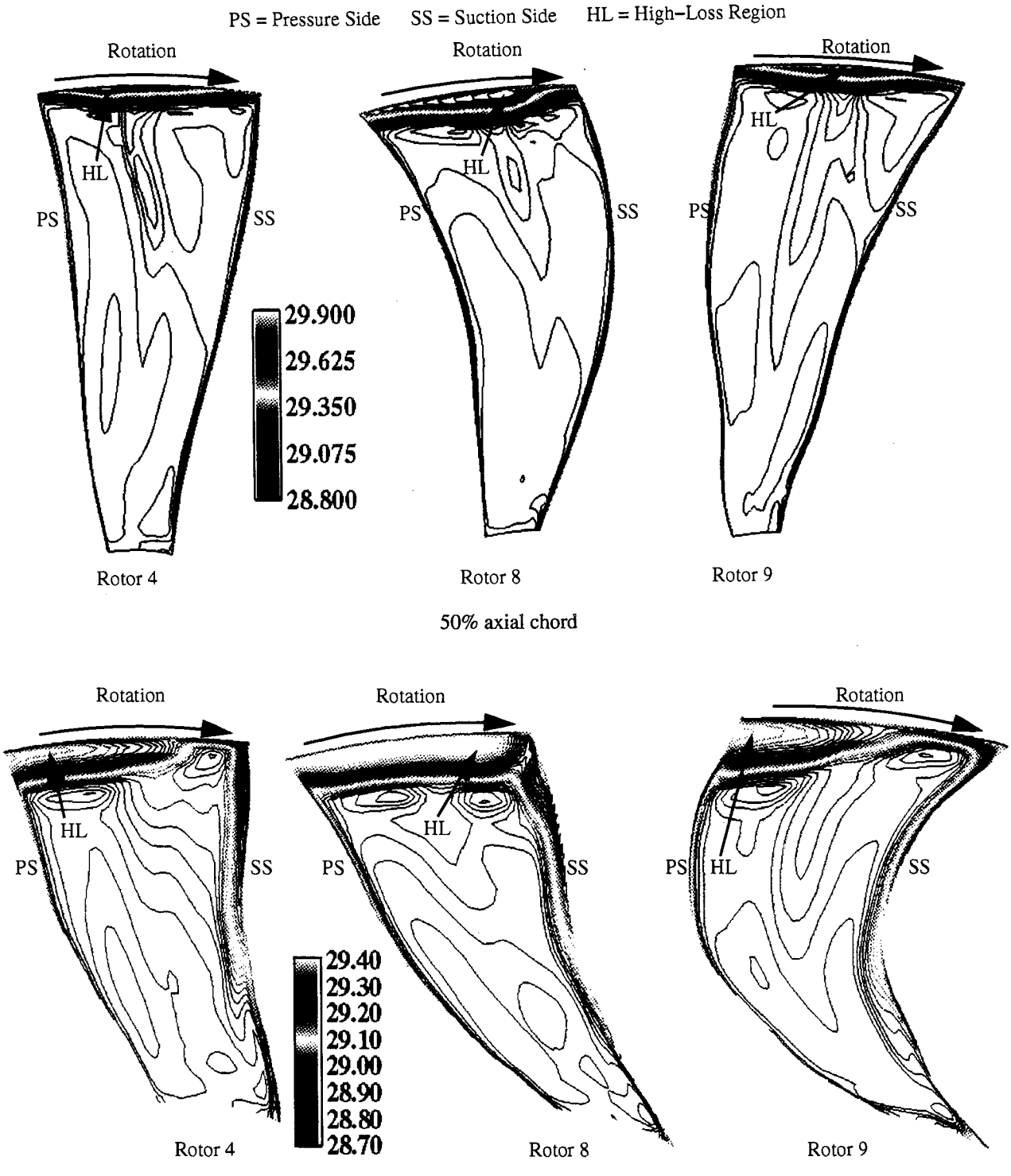

Fig. 22 Generation of entropy at design speed near peak-efficiency.

REFERENCES

Beatty, L. A., Savage, M., and Emery, J. C., 1954 "Low Speed Cascade Tests of Two 45 Degree Swept Compressor Blades with Constant Spanwise Loading," NASA Research Memorandum, L53L07.

Bliss, D. B., Hayden, R. E., Murray, B. S., and Schwaar, P. G., 1976, "Design Considerations for a Novel Low Source Noise Transonic Fan Stage," AIAA Paper 76-577.

Copenhaver, W. W., Hah, C., and Puterbaugh, S. L., 1993, "Three-Dimensional Flow Phenomena in a Transonic High-Through-Flow Compressor Stage," ASME Journal of Turbomachinery, Vol. 115, pp. 240-248.

Gostelow, J. P. and Smith, L. H., 1968, "Aerodynamic Design and Performance of a Swept Back Rotor SW-1," GE Internal Report 68-AEG -175.

Hah, C., Puterbaugh, S. L., 1991, "A Critical Evaluation of a Three-Dimensional Navier-Stokes Method as a Tool to Calculate Transonic Flows inside a Low-Aspect-Ratio Compressor," AGARD-CP-510, CFD Techniques for Propulsion Applications.

Hah, C., and Wennerstrom, A.J., 1991, "Three-Dimensional Flow Fields inside a Transonic Compressor with Swept Blades," ASME Journal of Turbomachinery, Vol. 113, No. 1, pp. 241-251.

Hayden, R. E., Bliss, D. B., Murray, B. S., Chandiramani, K. L., Smillin, J. I., and Schwaar, P. G., 1978, "Analysis and Design of a High Speed Low Noise Aircraft Fan Incorporating Swept Leading Edge Rotor and Stator Blade," NASA CR-135092.

Law, C. H. and Wadia A. R., 1993, "Low Aspect Ratio Transonic Rotors, Part 1: Baseline Design and Performance," ASME Journal of Turbomachinery, Vol. 115, pp. 218-225.

Lewis R. I. and Hill, J. M., 1971, "The Influence of Sweep and Dihedral in Turbomachinery Blade Rows," Journal of Mechanical Engineering Science, Vol. 13, No. 4.

Mohammed, K. P. and Prithviraj, D., 1977, "Investigation on Axial Flow Fan Impeller with For-ward-swept Blades," ASME Paper 77-FE-1.

Newbert, R. J., Hobbs, D. E., and Weingold, H. D., 1990," Application of Sweep to Improve the Efficiency of a Transonic Fan, Part-1 Design," AIAA Paper 90-195.

Prince, D. C. Jr., 1980," Three-Dimensional Shock Structures for Transonic/Supersonic Compressor Rotors," Journal of Aircraft, Vol. 17, No. 1, pp. 28-37.

Rabe, D., Hoying, D., and Koff, S., 1991, "Application of Sweep to Improve Efficiency of a Transonic Fan, Part-2 Performance and Laser Test REsults, "AIAA Paper 91-2540.

Smith, L. H. and Yeh, H., 1963, "Sweep and Dihedral Effect in Axial Flow Turbomachinery," ASME Journal of Basic Engineering, Vol. 85.

Yamaguchi, N., Tominaga, T., Hattori, S. and Mitsubishi, T, 1991, "Secondary-Loss Reduction by Forward-Skewing of Axial Compressor Rotor Blading," Proceedings of 1991 Yokohama International Gas turbine Congress, Vol. 2, pp. 61-68.

Wadia, A. R., Szucs, P. N. and Crall, D. W., 1997 "Inner Workings of Aerodynamic Sweep," ASME Paper 97-GT-401.

Wadia, A. R., Copenhaver, W. W., 1996 "An Investigation of the Effect of Cascade Area Ratios on Transonic Compressor Performance," ASME Journal of Turbomachinery, Vol. 118.

Wennerstrom, A.J. and Puterbaugh, S. L., 1984, "A Three-Dimensional Model for the Prediction of Shock Losses in Compressor Blade rows," ASME Journal of Engineering for Gas Turbines and Power, Vol. 106, No. 2, pp. 295-299.